Title

Locus coeruleus volume and cell population changes during Alzheimer's disease progression: A stereological study in human postmortem brains with potential implication for early-stage biomarker discovery

Permalink

https://escholarship.org/uc/item/11k044pf

Journal

Alzheimer's & Dementia, 13(3)

ISSN

1552-5260

Authors

Theofilas, Panos
Ehrenberg, Alexander J
Dunlop, Sara
et al.

Publication Date

2017-03-01

DOI

10.1016/j.jalz.2016.06.2362

Peer reviewed

Locus coeruleus volume and cell population changes during Alzheimer's disease progression: a stereological study in human postmortem brains with potential implication for early-stage biomarker discovery

Panos Theofilas, PhD[1], **Alexander J. Ehrenberg**[1], **Sara Dunlop, BS**[1], **Ana T. Alho, PhD**[2,3], **Austin Nguy**[1], **Renata Elaine Paraizo Leite, PhD**[3], **Roberta Diehl Rodriguez, MD**[3], **Maria B. Mejia, BS**[1], **Claudia K. Suemoto, MD, PhD**[3], **Renata Eloah de Lucena Ferretti-Rebustini, PhD**[4], **Livia Polichiso, BS**[3], **Camila F. Nascimento, PhD**[3], **William W. Seeley, MD, PhD**[1], **Ricardo Nitrini, MD, PhD**[3], **Carlos Augusto Pasqualucci, MD, PhD**[3], **Wilson Jacob Filho, MD, PhD**[3], **Udo Rueb, MD, PhD**[5], **John Neuhaus, PhD**[1], **Helmut Heinsen, MD, PhD**[3,6], and **Lea T. Grinberg, MD, PhD**[1,3]

[1]University of California, San Francisco, San Francisco, CA, USA

[2]Hospital Albert Einstein, São Paulo, Brazil

[3]University of São Paulo Medical School, São Paulo, Brazil

[4]University of São Paulo, School of Nursing, São Paulo, Brazil

[5]University of Frankfurt, Frankfurt, Germany

[6]University of Wuerzburg, Wuerzburg, Germany

Abstract

Introduction—Alzheimer's disease (AD) progression follows a specific spreading pattern, emphasizing the need to characterize those brain areas that degenerate first. The brainstem's locus coeruleus (LC) is the first area to develop neurofibrillary changes (NFT).

Methods—Unbiased stereological analyses in human brainstems to estimate LC volume and neuronal population in controls and individuals across all AD stages.

Results—As the Braak stage increases by 1 unit, the LC volume decreases by 8.4%. Neuronal loss started only midway through AD progression. Age-related changes spare the LC.

Discussion—The long gap between NFT accumulation and neuronal loss suggests that a second trigger may be necessary to induce neuronal death in AD. Imaging studies should determine whether LC volumetry can replicate the stage-wise atrophy observed here and how

Corresponding author: Lea Tenenholz Grinberg, MD/PhD, Associate Professor in Residence, Memory and Aging Center, Department of Neurology, Sandler Neurosciences Center, Box 1207, 675 Nelson Rising Lane, Room 211B, San Francisco, CA 94158, Phone: 415-502-7174, Fax: 415-476-5573, lea.grinberg@ucsf.edu.

these changes are specific to AD. LC volumetry may develop into a screening biomarker for selecting high-yield candidates to undergo expensive and less accessible PET-scans and to monitor AD progression from pre-symptomatic stages.

Keywords

Alzheimer's disease; brainstem; locus coeruleus; human; neurofibrillary tangles; unbiased stereology; postmortem; neuron counts; volumetry

1. Introduction

The UN projects that more than 200 million people will suffer from neurodegenerative diseases by 2050. In the USA alone, the cost of dementia is over $160 billion a year and is projected to reach $1.1 trillion by 2050 [1]. Effective disease-modifying treatments for AD remain elusive. In recent years, all promising therapies for AD that appeared efficacious in animal models fell short when tested in humans [2]. Oversimplification and incomplete modeling of AD pathophysiology are, at least partly, to blame for this failure [3]. AD features double-nature lesions. Besides accumulation of neuritic plaques and neurofibrillary tangles (NFTs), neuronal loss plays a critical role [4]. If fact, neuronal loss is considered the best correlate of cognitive deterioration in AD [5]. Furthermore, AD follows a predictable anatomical sequence, with lesions spreading along specific neuronal pathways [6]. Understanding the pathobiology of AD in the brain areas that degenerate first is critical for developing treatments to halt the spread of AD before it causes an irrevocable neuronal loss. Braak and Braak (BB) designed a universally used 7-point system for staging AD that recapitulates the stereotypical spreading pattern of tau cytoskeletal pathology in the cortex [7]. NFTs limited to transentorhinal/entorhinal cortex and hippocampus represent stages I/II. In 2009, our group demonstrated that tau cytoskeletal pathology in the dorsal raphe nucleus (DRN), a serotonin-producing nucleus in the midbrain, precedes the development of NFTs in transentorhinal cortex [8]. Re-examination of the temporal involvement of subcortical structures in AD followed [9,10], including Braak's group revision of their classical staging system in 2011 which now incorporates brainstem structures as precortical staging a-c [11]. They demonstrated that the locus ceruleus (LC), a noradrenergic nucleus located at the pons, shows NFTs as early as the fourth decade of life, corroborating previous findings of early LC involvement in AD [12–14]. The LC belongs to the isodendritic core, a phylogenetically conserved nuclei network [14]. NFT development in components of the isodendritic core consistently precedes NFTs in any cortical areas [8,10,11].

Understanding the changes in LC associated with AD progression may represent a window of opportunity for identifying biomarkers to detect AD in prodromal stages and inform on therapeutic targets to halt AD progression. Meticulous neuropathological investigations that could be criticized as "descriptive" were critical for creating the necessary foundation for further studies utilizing cutting-edge methods such as proteomics, high-resolution imaging, and improved animal models that advance the understanding of neurodegenerative diseases. Aiming to understand the impact of AD in the LC, we utilized design-based stereology to investigate LC volume and neuronal population changes in a sample of 68 subjects, enriched for controls and early AD stages.

2. Participants and methods

2.1 Participants

The majority of the cases (65) was sourced from the Brain Bank of the Brazilian Brain Aging Study Group (BBBABSG [15,16]). The Neurodegenerative Disease Brain Bank (NDBB) from the University of California, San Francisco (UCSF) supplied three cases (#62, 63, 68; Table 1). The institutional review boards of both participating institutions approved this study. The BBBABSG is supplied by the São Paulo City Autopsy Service (SPAS). Autopsies are mandatory for determining the cause of death in Sao Paulo and the SPAS performs approximately 13,000 autopsies are performed per year. All cases autopsied during morning hours are candidates for the BBBABSG after donation by next-of-kin [15]. The BBBABSG receives approximately 300 cases per year. A random rotation list among the studies supplied by the BBBABSG was created to accommodate all the studies requiring a modified protocol, including this one. For the current study, we received cases collected from 2010 to 2013. The NDBB receives brain and spinal cord donations from patients enrolled in the UCSF Memory and Aging Center. The great majority of UCSF/NDBB cases developed late-stage dementia, and most of the cases show more than one neurodegenerative condition. We collected the first three consecutive cases meeting the study criteria. The selection criteria for both centers included the absence of non-AD related neurodegenerative pathology or significant cerebrovascular lesions and availability of an intact brainstem. Subjects were excluded if they had a history of seizures, other neurological diseases, a primary Axis 1 psychiatric diagnosis, or gross non-degenerative structural pathology. For all cases, the neuropathological assessment was based on analysis of dementia-related structures embedded in paraffin wax, cut into 8-micron thick sections, and stained with immunohistochemistry. BBBABSG and NDBB neuropathological protocols are similar. AD pathology was staged according to the new NIA-AA guidelines [17]. Cases were categorized by the BB staging system for neurofibrillary changes [7]. Subjects were considered to be BB stage 0 or free of cortical NFTs when at least 4 sections across the transentorhinal cortex were negative for phospho-tau immunostaining (CP-13, gift of Peter Davies) [8]. Approximately 500 cases were screened for this study.

2.2. Tissue processing and staining

The tissue processing and staining methods used in this study have been previously described [18]. Briefly, each brainstem block was separated from the brain, fixed in 10% formalin, and embedded in 8% celloidin for subsequent sectioning [19]. Blocks were sectioned horizontally in serial sets, each one containing one 300-μm thick and five 60-μm thick sections. For cytoarchitectonic visualization of the LC, all odd-numbered sections were stained with gallocyanin-chromalum. Parallel sections were immunostained for phospho-tau (CP-13) after antigen retrieval [18]. Selected sections were immunostained for tyrosine hydroxylase (TH, 1:00, Millipore, Billerica, MA) for assisting with the LC border segmentation [18](Figure 1).

2.3. Stereological analyses

Stereological analyses of unilateral LC neuronal population were performed using the optical fractionator probe of the StereoInvestigator software (MBF StereoInvestigator v.10,

MBF Bioscience, Williston, VT, USA) [18]. LC borders were traced based on the Atlas of the Cytoarchitecture of the Human Brain Stem [20]: the LC lies rostrally in the caudal portion of the inferior colliculus and ends caudally to the motor nucleus of the trigeminal nucleus. We segmented the LC volume and estimated the neuronal population on the gallocyanin-stained thick sections. This stain allowed for a precise and consistent identification of the LC boarders, and the inclusion of non-TH positive mid- and large-size neurons. We estimated the neuronal population of the left LC in 63 cases (Tab. 1) using a 40× magnification objective (Plan-Apochromat 40x/1.30 oil objective, Zeiss) in all odd-numbered sections (~20–25) crossing the LC. Optimal stereological parameters were determined using the 'resample-oversample' analysis probes included in the StereoInvestigator software. Based on the output [18], we adopted a 13,828.1 μm^2 counting frame area and 421,515.0 μm^2 sampling grid area. The guard zone was established at 20 μm and dissector height at 90 μm. The coefficient of error (CE) range was calculated following Gundersen's and Schmitz-Hof's methods [21,22]. All pigmented and non-pigmented mid- and large-size neurons were included in the estimations. We used a BB 0 case to estimate the proportion of pigmented neurons using the same parameters.

The unilateral LC volumes were calculated for the 68 cases using the Cavalieri principle and the planimetry probe of the StereoInvestigator software, following manual delineation of the LC borders. For detecting a possible topographical gradient of vulnerability to AD across the disease progression, we subdivided the LC into equal rostral, middle, and caudal segments.

2.4. Statistical Analyses

The association of BB stage with the total LC population counts and volumes, and region-specific counts and volumes, were assessed using linear regression models, associated scatterplots, and lowess curves [23]. Scatterplots of LC volumes versus BB stage indicated that volumes varied linearly with BB stage. Therefore, we fitted regression models that included as predictors a linear term for BB stage, as well as age, gender and brain weight as potential confounding variables. The regression coefficient of BB stage in these models assessed the change in volume associated with an increase of one BB stage. The LC population counts versus BB stage exhibited a curvature that was accommodated by including linear and quadratic BB stage terms in the regression models. The models also included age, gender, and brain weight as potential confounding variables. In the quadratic models, the change in LC population counts associated with an increase of one BB stage depended on the stage. Thus, BB-stage-specific rates of change in LC population counts were calculated using the estimated derivative of the quadratic curve with respect to BB stage, along with associated 95% confidence intervals. The association of age with total LC population counts and volumes among the subjects in BB stages 0-I was assessed using linear regression models. LC population counts and volumes versus age indicated that both outcomes varied linearly with age, therefore we fit regression models that included as predictors a linear term for age, as well as BB stage, gender, and brain weight as potential confounding variables. Statistical analyses were conducted using the Stata software package (Stata Statistical Software v13, StataCorp, TX). In all tests, $p < 0.05$ denoted a significant difference.

3. Results

Table 1 summarizes demographics, morphological data, and cognitive status of all cases (47% females; mean age at death: 62.8 ± 10.3 years, range 44 to 96 years old).

3.1. Reductions in LC volume for each increment of the Braak and Braak stage

LC volume varied from 5.8 to 21.7 mm^3 (mean: 12.8 mm^3) and showed no significant gender differences (Figure 1C–D). Unadjusted linear regression models indicate a statistically significant correlation between a higher BB stage and smaller LC volume ($\beta = -0.853$; p<0.001; 95% coefficient interval (CI): [−1.27, −0.43]) Adjustment for gender, age, years of education, and brain weight increased the magnitude of the estimated regression coefficient to a $\beta = -1.078$ with p<0.001 and 95% CI: [−1.6, −0.6] (Figure 2A), which signifies as the BB stage increases by 1 unit, the average LC volume decreases by 1.08 mm^3, or 8.4% (Figure 2A). Significant volume reductions were also observed for each LC subregion (63 cases; Table 1). The magnitudes of the regression coefficients for rostral and middle LC were −0.407 (p<0.001; 95% CI: [−0.6, −0.2]) and −0.483 (p<0.001; 95% CI: [−0.7, −0.2]) per increment of BB stage, respectively, whereas the caudal part showed a smaller coefficient of −0.175 (p=0.031; 95% CI: [−0.3, −0.2]). Following adjustments, the coefficient values increased to −0.436 (p=0.001; 95% CI: [−0.7, −0.2]), −0.556 (p<0.001; 95% CI: [−0.8, −0.2]) and −0.193 (p=0.045; 95% CI: [−0.4, −0.0]) respectively (Figure 2B–D).

3.2. LC neuronal population only decreases from mid- Braak and Braak stages

Unbiased stereological estimates of the total LC cell population ranged between 6,674 to 137,910 cells (mean: 48,907 cells). The average CE was 0.07 for both the Gundersen's and Schmitz-Hof's methods, indicating high sampling precision [21,22]. Pigmented neurons corresponded to 46% of the total mid- and large-size LC cell population (Figure 3). Analyses adjusted for age, gender, years of education, and brain weight indicated relatively stable total LC population estimates in BB stages 0–II, with no statistical differences to BB 0 at 95% confidence intervals (Figure 4A). On the other hand, the rates of change in stages BB III–VI were negative and statistically significant.

The same pattern observed for the total LC neuronal population was seen in the rostral, middle, and caudal portions (Figure 4B–D). For the rostral LC neuronal population (Figure 4B), the rate of change at stage III was negative, but not statistically significant at the 5% level.

3.3. Normal aging does not affect LC volume and neuron population

To address if the differences observed in the LC could be partly attributed to age-related processes, we compared estimated LC volume and neuronal population in the subset of individuals at BB stages 0 and I (n=40; all CDR=0; 17 females; age range: 47–83 years; Table 1). Linear regression models using age as the primary predictor, along with gender and brain weight as potential confounding variables, showed no significant association between normal aging and changes in the LC (Figure 5).

3.4. Age, gender, brain weight, and years of education did not have statistically significant independent associations with the LC vulnerability in progressive stages of AD

We assessed the association between the BB stage, LC volume, and neuronal estimates, and demographics using linear regression and correlation analysis. We failed to find any correlation between age, gender, brain weight, or years of education as predictors of changes in LC.

4. Discussion

We used unbiased design-based stereology to analyze the LC volume in 68 brainstems and estimate the number of LC neurons in 63 brainstems, distributed through BB stages 0–VI and free from non-AD brain changes. Our observations produced four major findings. First, for each unit increment of the BB staging system the average LC volume reduced by 8.4%, starting in Braak 0. Second, despite this early volumetric shrinkage, the average neuronal dropout started at a much later stage, midway through the AD progression. Third, the caudal LC third showed fewer AD-related changes, suggesting a gradient of vulnerability within the nucleus. Fourth, normal aging did not significantly affect the LC, suggesting that our findings are likely related to the progression of AD pathology.

Anatomically, the LC two columns are located in the dorsolateral pontine tegmentum [20]. Being the major site of norepinephrine (NE) synthesis in the brain [24], the LC is crucial for regulating the sleep-wakefulness cycle [25,26], and behavioral responses such as depression and stress [27]. Studies dating back to the 1960s pointed to the early LC vulnerability to AD [12,13,28–31]. Furthermore, the importance of LC in AD is highlighted by studies in animal models showing that LC vulnerability to NFT followed by reduced NE availability in the brain mediate neurotoxicity, neuroinflammation, cognitive deficits, changes in neuronal metabolism, and blood-brain-barrier permeability in both human and experimental models [32–34]. In fact, we identified phospho-tau positive cytoplasmic inclusions in the LC of all cases, including the 18 cases at BB 0 corroborating previous suggestions that the high proportion depression, anxiety, and sleep disturbances seen often in prodromal AD may be mediated by AD changes in the isodendritic core [35,36].

To our knowledge, this is one of the few studies addressing the LC volumetric differences in AD and the first to report a linear volumetric reduction during AD early stages. Hoogendijk et al. reported a 22% LC volume difference between 5 AD and 5 control cases [37]. Had we dichotomized the cases, our findings would be similar. German et al. also implied that LC shrinks in AD based on dichotomous analyses of 8 AD and 7 controls [38]. We detected a significant linear decline of LC volume of 8.4% per BB stage increment beginning at the transition from BB 0 to BB I. This volumetric loss was significant in all the LC thirds. Although, a higher number of mid-stage cases would be necessary to clarify the rate of LC volume loss in AD mid-stages, we employed locally weighted regression that describe the local association of each BB stage increment with LC volume. Therefore, the observed decreased in volume between BB stages 0-I and I-II were independent on data in BB stages III-VI. Our findings indicate that LC volume shrinks by an average of 25% before the onset of AD-defining symptoms, which usually coincide with BB stage III. Further studies are necessary to determine the cause of this volumetric shrinkage.

Advances in neuroimaging are enabling *in vivo* volumetric studies of small brain regions [39] including the LC [40]. If imaging volumetry will be able to replicate the stage-wise LC atrophy observed at least in the early stages of AD, and these changes prove to have a high predictive value to AD, LC volumetry may translate into a powerful, scalable, and economic serial screening biomarker to guide workup decisions in AD. Consequently, LC volumetric changes could be the initial screening step required for selecting high-yield candidates to undergo less accessible and more expensive PET-scans. Furthermore, monitoring changes in LC volume may potentially be an end-point parameter for testing the efficacy of interventions against AD at individual level. This would be especially relevant during AD prodromal stages, as a decrease in volume can be probably detected years before the onset of clinical defining symptoms.

We detected a broad variability in LC population estimates within each BB stage (Figure 4) as anticipated from other studies [41]. Previous studies estimated unilateral LC neuronal population size of 12,000 to 60,000 cells in controls individuals. Several factors may explain the discrepancy among the studies. Unbiased stereological methods are tedious, labor-intense, and, most importantly, rely on the availability of the whole volume of interest. Only a fraction of LC studies employed unbiased stereological methods [37,42,43]. Here, using an advanced stereology set-up, it took 1260 hours of counting to estimate the unilateral population size of all LC. To avoid redundant work, we used a oversample-resample approach to set the paraments [18]. Curiously, when minimally decreasing the sampling size, we obtained over 50% differences in estimations, despite the fact that CE values were acceptable (< 0.1) in both cases. In fact, a low CE is an indicator rather than a guarantee of unbiased estimations[22]. The neuronal types included in the estimate is another source of discrepancies. We included all mid- and large-size LC neurons, whereas many studies restricted the counts to TH-positive or neuromelanin-bearing neurons [31,38,42–46]. According to ours and others estimations [20,44], pigmented neurons correspond to approximately 3/5 of the total mid- and large-size LC neurons in controls.

Regardless of the method employed, all studies point to a significant LC neuronal loss in AD [14]. This study though, innovates by classifying the cases using the 7-point BB staging system rather than in a dichotomized manner, thus informing when in the process the neuronal loss starts. Unexpectedly, despite strong evidence of tau cytoskeletal pathology and a linear LC volume decrease from BB stage 0, differences in LC neuronal population became significant and conspicuous only from BB stage III. In a recent study, Arendt et al. [31] also reported a delay in significant LC neuronal loss based on 119 LC classified into four clinicopathological groups. Together, our studies point to a large gap between the apparance of tau cytoskeletal pathology and neuronal loss in humans [5]. It is noteworthy that subject #63 (Table 1; BB stage VI) has less than 1/3 of the average number of neurons than the other BB stage VI cases, despite being younger. This corroborate suggestions that early-onset AD is more aggressive than late-onset AD, despite sharing identical neuropathological hallmarks [47]. In fact, NFTs and neuritic plaques are not always a surrogate marker of neuronal loss [5]. Investigations focusing on mechanisms to protect neurons from NFT-related toxicity may potentially disclose relevant targets for disease-modifying treatment [48]. Experimental studies demonstrating that norepinephrine restoration slows of neurodegeneration, situate the LC as a relevant area to research

investigating protective mechanisms against AD [49]. Similarly, studies in the LC may disclose possible second hit mechanisms necessary to trigger neuronal loss in NFT-bearing neurons.

Agreeing with previous studies [37,38,44–46], we observed a selective LC topographical vulnerability to AD with the rostral and middle thirds more vulnerable than the caudal third. Again, the novelty here was to identify at which point in the disease process and at what rate this regional neuronal loss happens. Such topographical inhomogeneity in LC vulnerability corroborates a network-based, bi-directional spread of AD [50]. For instance, unilateral injection of synthetic tau into the LC of young PS19 mice overexpressing mutant human tau induced neuronal loss from the ipsilateral LC, and significant tau pathology in brain regions anatomically connected with the LC. Reversely, synthetic tau injections into cortical regions rapidly induced pathogenesis in the LC [51]. In rodents and monkeys, the LC rostral and middle parts project to and receive inputs from cortical, diencephalic, and forebrain structures [46,52,53], found especially vulnerable to AD in humans. The relatively spared caudal pole is reciprocally connected with regions unaffected in AD, including spinal cord and cerebellum [54]. These findings also highlight the importance of anatomical precision in tissue sampling for biochemical and molecular studies for avoiding false results.

The brain shows a sub-regional vulnerability to normal aging processes [55]. To address if aging could be a confounder to our results, we analyzed the LC volume and neuron population size of the 40 BB stage 0 or I individuals. The LC volume and neuronal population remained stable throughout the age groups, suggesting that the changes observed in the LC were AD-related. This is in partial contrast with previous reporting none to up to 50% loss of the LC neurons in older individuals [43,45,56,57]. Here again, methodological differences including lack of unbiased methods for estimating neuronal counts could explain the discrepancies [43,45,56–58]. Additionally, lack of power [56–58] or unequal gender distribution [43,45] could also have influenced some of these studies.

This study has a considerable strengths. It relies on a relatively large sample of cases free of non-AD changes that minimize confounders caused by other diseases. Additionally, it brings unparalled number of controls and early AD cases. The age range of our samples is more similar to the individuals at-risk for having prodromal AD than most of the other series. Finally, we took several steps to ensure an unbiased analyses. We employed unbiased stereology in thick, gallocyanin-stained serial sections. This staining penetrates fully into the tissue and provides excellent signal-to-noise ratio (Fiure 1A), resulting in a great tool to visualize cytoarchitectonic features of all neuronal subtypes [18]. Certain limitations in this study ought to be mentioned. A cross-sectional analysis does not exclude the possibility of an alternative outcome had we chosen another time frame. Also, our estimations may contain bias due to various factors that cannot be controlled, including agonal changes. Regarding the effects of normal aging on LC, we cannot exclude the possibility that LC would change in the "oldest-old". Unilateral counting increased time efficiency. However, we cannot rule out that bilateral counts of the LC may change our results. Finally, although the method employed for estimating neuronal numbers is not affected by tissue shrinkage, the volume estimations could potentially be. To minimize errors due process-related

shrinkage [22], we employed methods that cause less distortion than traditional neuropathological methods [18].

In conclusion, our findings suggest that accumulation of tau cytoskeletal pathology and significant volumetric changes precede neuronal loss in the LC during AD progression. Further studies are necessary to investigate which processes protect from and correlate with the onset of LC neuronal death in AD. From an early diagnostic perspective, future *in vivo* imaging studies should determine whether LC volumetry could replicate the stage-wise atrophy shown here, what are the predictive value of these changes to AD pathology and provide a screening and monitoring biomarkers to AD.

Acknowledgments

References

1. Hurd MD, Martorell P, Langa KM. Monetary costs of dementia in the United States. N Engl J Med. 2013; 369:489–490. [PubMed: 23902508]

2. Iqbal K, Liu F, Gong CX. Alzheimer disease therapeutics: focus on the disease and not just plaques and tangles. Biochem Pharmacol. 2014; 88:631–639. [PubMed: 24418409]

3. Korczyn AD. Why have we failed to cure Alzheimer's disease? J Alzheimers Dis. 2012; 29:275–282. [PubMed: 22258512]

4. Duyckaerts C, Delatour B, Potier MC. Classification and basic pathology of Alzheimer disease. Acta Neuropathol. 2009; 118:5–36. [PubMed: 19381658]

5. Andrade-Moraes CH, Oliveira-Pinto AV, Castro-Fonseca E, da Silva CG, Guimaraes DM, Szczupak D, Parente-Bruno DR, Carvalho LR, Polichiso L, Gomes BV, Oliveira LM, Rodriguez RD, Leite RE, Ferretti-Rebustini RE, Jacob-Filho W, Pasqualucci CA, Grinberg LT, Lent R. Cell number changes in Alzheimer's disease relate to dementia not to plaques and tangles. Brain. 2013; 136:3738–3752. [PubMed: 24136825]

6. Seeley WW, Crawford RK, Zhou J, Miller BL, Greicius MD. Neurodegenerative diseases target large-scale human brain networks. Neuron. 2009; 62:42–52. [PubMed: 19376066]

7. Braak H, Braak E. Neuropathological stageing of Alzheimer-related changes. Acta Neuropathol. 1991; 82:239–259. [PubMed: 1759558]

8. Grinberg LT, Rub U, Ferretti RE, Nitrini R, Farfel JM, Polichiso L, Gierga K, Jacob-Filho W, Heinsen H. Brazilian Brain Bank Study Group, The dorsal raphe nucleus shows phospho-tau neurofibrillary changes before the transentorhinal region in Alzheimer's disease. A precocious onset? Neuropathol Appl Neurobiol. 2009; 35:406–416. [PubMed: 19508444]

9. Simic G, Stanic G, Mladinov M, Jovanov-Milosevic N, Kostovic I, Hof PR. Does Alzheimer's disease begin in the brainstem? Neuropathol Appl Neurobiol. 2009; 35:532–554. [PubMed: 19682326]

10. Stratmann K, Heinsen H, Korf HW, Del Turco D, Ghebremedhin E, Seidel K, Bouzrou M, Grinberg LT, Bohl J, Wharton SB, den Dunnen W, Rub U. Precortical phase of Alzheimer's disease (AD)-related tau cytoskeletal pathology. Brain Pathol. 2015 [PubMed: 26193084]

11. Braak H, Thal DR, Ghebremedhin E, Del Tredici K. Stages of the pathologic process in Alzheimer disease: age categories from 1 to 100 years. J Neuropathol Exp Neurol. 2011; 70:960–969. [PubMed: 22002422]

12. Tomlinson BE, Irving D, Blessed G. Cell loss in the locus coeruleus in senile dementia of Alzheimer type. J Neurol Sci. 1981; 49:419–428. [PubMed: 7217992]

13. Grudzien A, Shaw P, Weintraub S, Bigio E, Mash DC, Mesulam MM. Locus coeruleus neurofibrillary degeneration in aging mild cognitive impairment and early Alzheimer's disease. Neurobiol Aging. 2007; 28:327–335. [PubMed: 16574280]

14. Theofilas P, Dunlop S, Heinsen H, Grinberg LT. Turning on the Light Within: Subcortical Nuclei of the Isodentritic Core and their Role in Alzheimer's Disease Pathogenesis. J Alzheimers Dis. 2015 [PubMed: 25720408]

15. Grinberg LT, Ferretti RE, Farfel JM, Leite R, Pasqualucci CA, Rosemberg S, Nitrini R, Saldiva PH, Filho WJ. Brazilian Aging Brain Study Group. Brain bank of the Brazilian aging brain study group - a milestone reached and more than 1,600 collected brains. Cell Tissue Bank. 2007; 8:151–162. [PubMed: 17075689]

16. Ferretti RE, Damin AE, Brucki SMD, Morillo LS, Perroco TR, Campora F, et al. Post-Mortem diagnosis of dementia by informant interview. Dementia and Neuropsychologia. 2010; 4:138–144.

17. Montine TJ, Phelps CH, Beach TG, Bigio EH, Cairns NJ, Dickson DW, Duyckaerts C, Frosch MP, Masliah E, Mirra SS, Nelson PT, Schneider JA, Thal DR, Trojanowski JQ, Vinters HV, Hyman BT. National Institute on Aging, Alzheimer's Association. National Institute on Aging-Alzheimer's Association guidelines for the neuropathologic assessment of Alzheimer's disease: a practical approach. Acta Neuropathol. 2012; 123:1–11. [PubMed: 22101365]

18. Theofilas P, Polichiso L, Wang X, Lima LC, Alho AT, Leite RE, Suemoto CK, Pasqualucci CA, Jacob-Filho W, Heinsen H, Grinberg LT. Brazilian Aging Brain Study Group. A novel approach for integrative studies on neurodegenerative diseases in human brains. J Neurosci Methods. 2014; 226:171–183. [PubMed: 24503023]

19. Heinsen H, Arzberger T, Schmitz C. Celloidin mounting (embedding without infiltration) - a new simple and reliable method for producing serial sections of high thickness through complete human brains and its application to stereological and immunohistochemical investigations. J Chem Neuroanat. 2000; 20:49–59. [PubMed: 11074343]

20. Olszewski, J.; Baxter, D. Cytoarchitecture of the Human Brain Stem. 2. Karger; Basel ; New York: 1982.

21. Gundersen HJ, Jensen EB, Kieu K, Nielsen J. The efficiency of systematic sampling in stereology--reconsidered. J Microsc. 1999; 193:199–211. [PubMed: 10348656]

22. Schmitz C, Hof PR. Design-based stereology in neuroscience. Neuroscience. 2005; 130:813–831. [PubMed: 15652981]

23. CLEVELAND W. Lowess - a Program for Smoothing Scatterplots by Robust Locally Weighted Regression. American Statistician. 1981; 35:54–54.

24. Berridge CW, Waterhouse BD. The locus coeruleus-noradrenergic system: modulation of behavioral state and state-dependent cognitive processes. Brain Res Brain Res Rev. 2003; 42:33–84. [PubMed: 12668290]

25. Pace-Schott EF, Hobson JA. The neurobiology of sleep: genetics cellular physiology and subcortical networks. Nat Rev Neurosci. 2002; 3:591–605. [PubMed: 12154361]

26. Gompf HS, Mathai C, Fuller PM, Wood DA, Pedersen NP, Saper CB, Lu J. Locus ceruleus and anterior cingulate cortex sustain wakefulness in a novel environment. J Neurosci. 2010; 30:14543–14551. [PubMed: 20980612]

27. Sara SJ, Bouret S. Orienting and reorienting: the locus coeruleus mediates cognition through arousal. Neuron. 2012; 76:130–141. [PubMed: 23040811]

28. Ishii T. Distribution of Alzheimer's neurofibrillary changes in the brain stem and hypothalamus of senile dementia. Acta Neuropathol. 1966; 6:181–187. [PubMed: 5963288]

29. Mann DM, Yates PO, Marcyniuk B. Correlation between senile plaque and neurofibrillary tangle counts in cerebral cortex and neuronal counts in cortex and subcortical structures in Alzheimer's disease. Neurosci Lett. 1985; 56:51–55. [PubMed: 4011048]

30. Braak H, Del Tredici K. The pathological process underlying Alzheimer's disease in individuals under thirty. Acta Neuropathol. 2011; 121:171–181. [PubMed: 21170538]

31. Arendt T, Bruckner MK, Morawski M, Jager C, Gertz HJ. Early neurone loss in Alzheimer's disease: cortical or subcortical? Acta Neuropathol Commun. 2015; 3 10-015-0187-1. [PubMed: 25853173]

32. Feinstein DL, Heneka MT, Gavrilyuk V, Dello Russo C, Weinberg G, Galea E. Noradrenergic regulation of inflammatory gene expression in brain. Neurochem Int. 2002; 41:357–365. [PubMed: 12176079]

33. Weinshenker D. Functional consequences of locus coeruleus degeneration in Alzheimer's disease. Curr Alzheimer Res. 2008; 5:342–345. [PubMed: 18537547]

34. Heneka MT, Nadrigny F, Regen T, Martinez-Hernandez A, Dumitrescu-Ozimek L, Terwel D, Jardanhazi-Kurutz D, Walter J, Kirchhoff F, Hanisch UK, Kummer MP. Locus ceruleus controls Alzheimer's disease pathology by modulating microglial functions through norepinephrine. Proc Natl Acad Sci U S A. 2010; 107:6058–6063. [PubMed: 20231476]

35. Hahn EA, Wang HX, Andel R, Fratiglioni L. A change in sleep pattern may predict Alzheimer disease. Am J Geriatr Psychiatry. 2014; 22:1262–1271. [PubMed: 23954041]

36. Masters MC, Morris JC, Roe CM. "Noncognitive" symptoms of early Alzheimer disease: a longitudinal analysis. Neurology. 2015; 84:617–622. [PubMed: 25589671]

37. Hoogendijk WJ, Pool CW, Troost D, van Zwieten E, Swaab DF. Image analyser-assisted morphometry of the locus coeruleus in Alzheimer's disease, Parkinson's disease and amyotrophic lateral sclerosis. Brain. 1995; 118(Pt 1):131–143. [PubMed: 7894999]

38. German DC, Manaye KF, White CL 3rd, Woodward DJ, McIntire DD, Smith WK, Kalaria RN, Mann DM. Disease-specific patterns of locus coeruleus cell loss. Ann Neurol. 1992; 32:667–676. [PubMed: 1449247]

39. Teipel S, Heinsen H, Amaro E Jr, Grinberg LT, Krause B, Grothe M. Alzheimer's Disease Neuroimaging Initiative. Cholinergic basal forebrain atrophy predicts amyloid burden in Alzheimer's disease. Neurobiol Aging. 2014; 35:482–491. [PubMed: 24176625]

40. Deistung A, Schafer A, Schweser F, Biedermann U, Gullmar D, Trampel R, Turner R, Reichenbach JR. High-Resolution MR Imaging of the Human Brainstem In vivo at 7 Tesla. Front Hum Neurosci. 2013; 7:710. [PubMed: 24194710]

41. Lyness SA, Zarow C, Chui HC. Neuron loss in key cholinergic and aminergic nuclei in Alzheimer disease: a meta-analysis. Neurobiol Aging. 2003; 24:1–23. [PubMed: 12493547]

42. Zarow C, Lyness SA, Mortimer JA, Chui HC. Neuronal loss is greater in the locus coeruleus than nucleus basalis and substantia nigra in Alzheimer and Parkinson diseases. Arch Neurol. 2003; 60:337–341. [PubMed: 12633144]

43. Vijayashankar N, Brody H. A quantitative study of the pigmented neurons in the nuclei locus coeruleus and subcoeruleus in man as related to aging. J Neuropathol Exp Neurol. 1979; 38:490–497. [PubMed: 469568]

44. Chan-Palay V, Asan E. Alterations in catecholamine neurons of the locus coeruleus in senile dementia of the Alzheimer type and in Parkinson's disease with and without dementia and depression. J Comp Neurol. 1989; 287:373–392. [PubMed: 2570794]

45. Busch C, Bohl J, Ohm TG. Spatial temporal and numeric analysis of Alzheimer changes in the nucleus coeruleus. Neurobiol Aging. 1997; 18:401–406. [PubMed: 9330971]

46. Marcyniuk B, Mann DM, Yates PO. Loss of nerve cells from locus coeruleus in Alzheimer's disease is topographically arranged. Neurosci Lett. 1986; 64:247–252. [PubMed: 3960404]

47. Panegyres PK, Chen HY. Differences between early and late onset Alzheimer's disease. Am J Neurodegener Dis. 2013; 2:300–306. [PubMed: 24319647]

48. Robertson IH. A noradrenergic theory of cognitive reserve: implications for Alzheimer's disease. Neurobiol Aging. 2013; 34:298–308. [PubMed: 22743090]

49. Chalermpalanupap T, Kinkead B, Hu WT, Kummer MP, Hammerschmidt T, Heneka MT, Weinshenker D, Levey AI. Targeting norepinephrine in mild cognitive impairment and Alzheimer's disease. Alzheimers Res Ther. 2013; 5:21. [PubMed: 23634965]

50. Saper CB, Wainer BH, German DC. Axonal and transneuronal transport in the transmission of neurological disease: potential role in system degenerations including Alzheimer's disease. Neuroscience. 1987; 23:389–398. [PubMed: 2449630]

51. Iba M, McBride JD, Guo JL, Zhang B, Trojanowski JQ, Lee VM. Tau pathology spread in PS19 tau transgenic mice following locus coeruleus (LC) injections of synthetic tau fibrils is determined by the LC's afferent and efferent connections. Acta Neuropathol. 2015; 130:349–362. [PubMed: 26150341]

52. Samuels ER, Szabadi E. Functional neuroanatomy of the noradrenergic locus coeruleus: its roles in the regulation of arousal and autonomic function part I: principles of functional organisation. Curr Neuropharmacol. 2008; 6:235–253. [PubMed: 19506723]

53. Loughlin SE, Foote SL, Bloom FE. Efferent projections of nucleus locus coeruleus: topographic organization of cells of origin demonstrated by three-dimensional reconstruction. Neuroscience. 1986; 18:291–306. [PubMed: 3736860]

54. Westlund KN, Coulter JD. Descending projections of the locus coeruleus and subcoeruleus/medial parabrachial nuclei in monkey: axonal transport studies and dopamine-beta-hydroxylase immunocytochemistry. Brain Res. 1980; 2:235–264. [PubMed: 7470856]

55. Pfefferbaum A, Mathalon DH, Sullivan EV, Rawles JM, Zipursky RB, Lim KO. A quantitative magnetic resonance imaging study of changes in brain morphology from infancy to late adulthood. Arch Neurol. 1994; 51:874–887. [PubMed: 8080387]

56. Manaye KF, McIntire DD, Mann DM, German DC. Locus coeruleus cell loss in the aging human brain: a non-random process. J Comp Neurol. 1995; 358:79–87. [PubMed: 7560278]

57. Tomonaga M. Neuropathology of the locus ceruleus: a semi-quantitative study. J Neurol. 1983; 230:231–240. [PubMed: 6198483]

58. Chan-Palay V, Asan E. Quantitation of catecholamine neurons in the locus coeruleus in human brains of normal young and older adults and in depression. J Comp Neurol. 1989; 287:357–372. [PubMed: 2570793]

Research in Context

Systematic review

A review on the topic was published by us this year. Literature search was conducted using PubMed and the relevant citations are appropriately cited. Further background review was conducted via private discussions with specialist in the field.

Interpretation

Our results shed light into the first pathological changes caused by AD in humans. They highlight the importance of brainstem in AD and provide a foundation for studies focusing on biomarkers and drug discovery.

Future directions

The manuscript identified two novel patterns of AD-related changes in the LC that can directly impact diagnosis and treatment of AD. Future studies to confirm if imaging can replicate the stage-wise linear LC volumetric reduction shown here may transform LC volumetry in a non-invasive biomarker for detecting prodromal AD and monitoring interventions. Furthermore, studies focusing on 2nd hits triggering neuronal death in tangle-bearing neurons may identify disease-modifying strategies to minimize neuronal loss in AD.
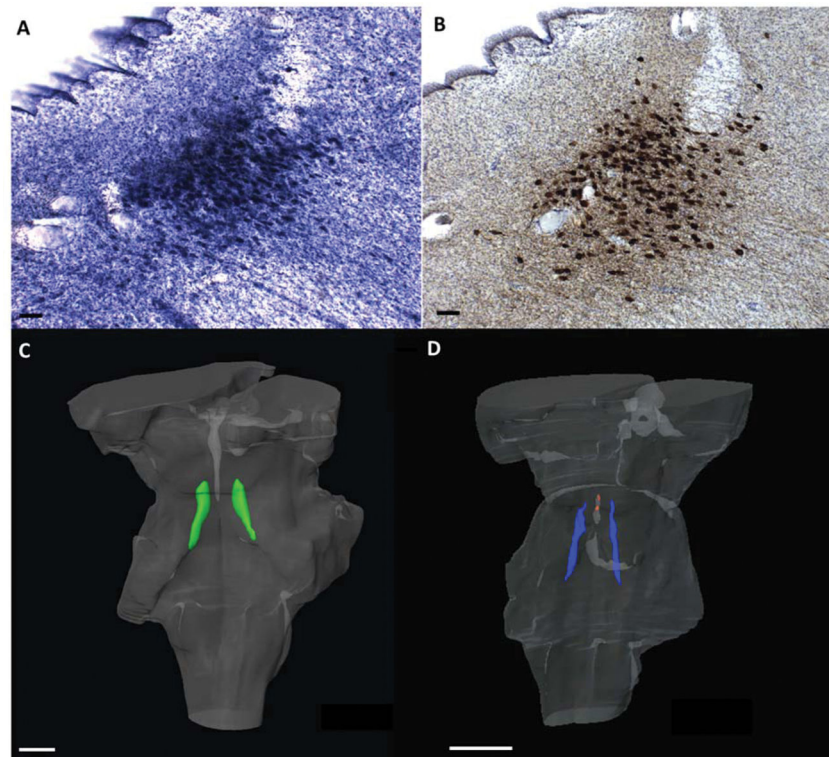
Figure 1.
300 μm-thick horizontal histological sections across the locus ceruleus (LC) in a control (Braak and Braak stage 0) subject, stained with gallocyanin (Nissl) (A) and immunostained for tyrosine hydroxylase (TH; B). LC border segmentation on the thick gallocyanin stained is comparable to the TH-immunostained sections and brings the advantage of including the TH-negative neurons. C and D) Volume reconstructions of the human brainstem (glass) and locus ceruleus (LC) in a Braak and Braak stage 0 subject (C) (LC in green), and in a Braak and Braak VI subject (D) (LC in blue). Note the conspicuous atrophy in B. Scale bars: 100 μm.
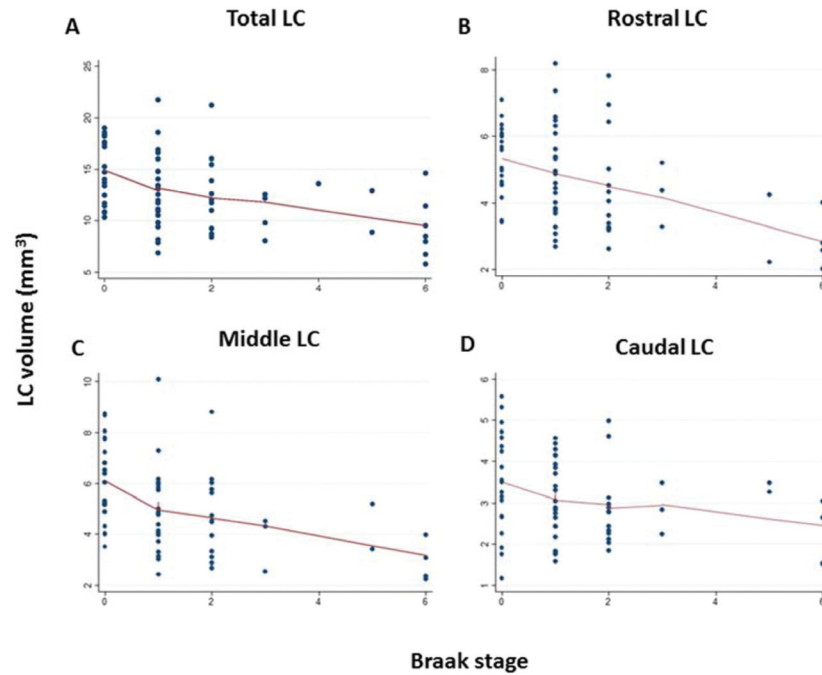
Figure 2.
Plots examining the association between Braak stages and neuronal volumes for the locus ceruleus (LC). Linear regression models indicate a negative correlation between Braak stage and total LC volume (A), with an estimated volume loss of 8.4% per BB stage increment (β = −1.078 with p<0.001 and 95% CI: [−1.6, −0.6]). Furthermore, a significant reduction of partial LC volumes was observed in all three subregions of the nucleus, including the rostral (B; β =−0.436; p=0.001; 95% CI: [−0.7, −0.2]), middle (C; β =− 0.556; p>0.001; 95% CI: [−0.8, −0.2]) , and caudal LC (D; β =− 1.193; p=0.045; 95% CI: [−0.4, −0.0]). The locally weighted regression (lowess) curves assess the local association of LC volumes with Braak stage using a bandwidth of 0.8 in Braak stage. Thus, the values of the lowess curves at Braak stage 0, I, II do not depend on data in Braak stages III–VI.

Figure 3.
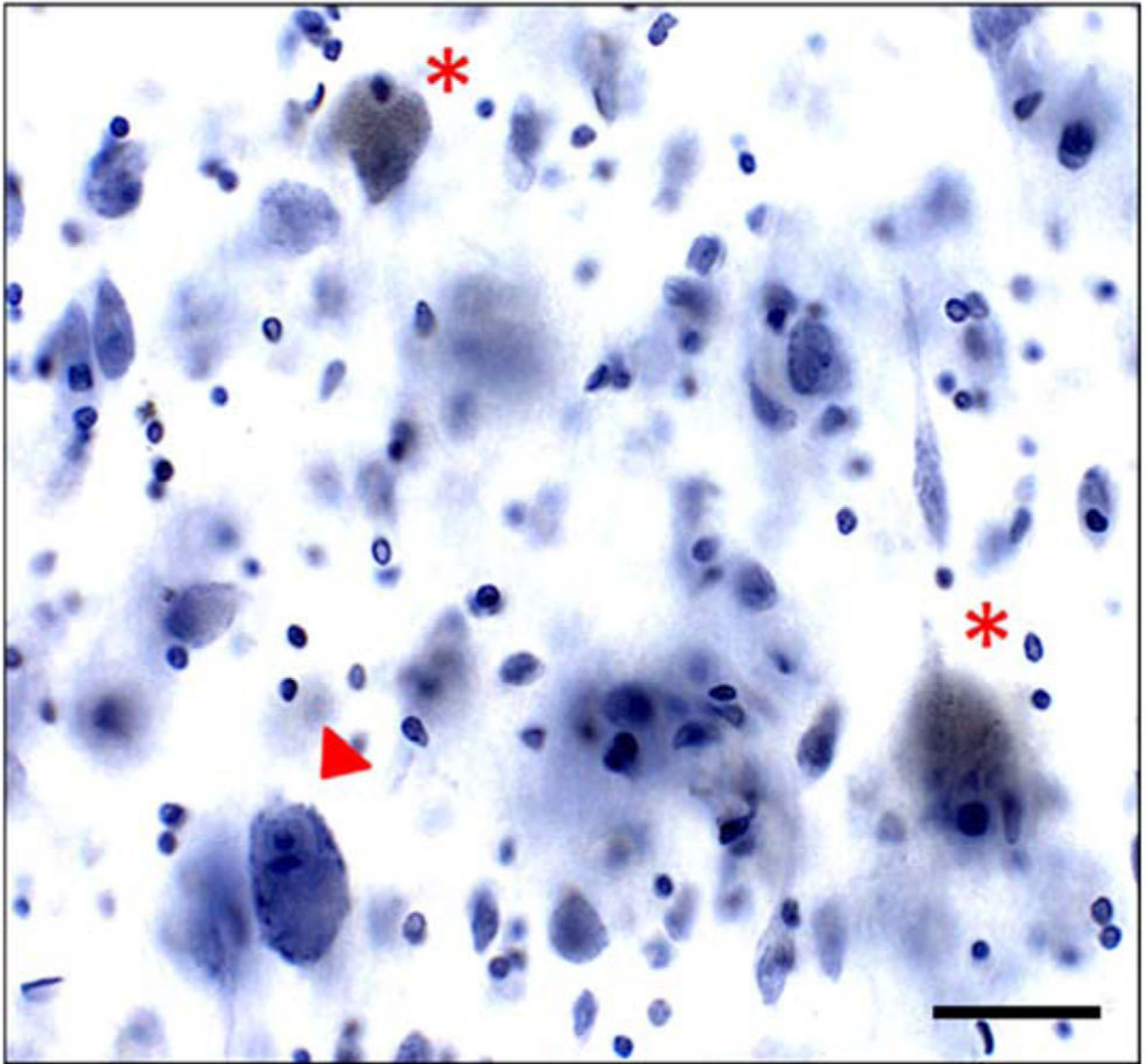Gallocyanin-stained neurons of the locus ceruleus (LC) showing a clearly distinct cytoplasm, an off-centered nucleus, and a darkly stained nucleolus, the last used as the counting reference for unbiased stereological analyses of the LC population estimates. The LC includes a collection of large and middle-sized neurons with melanin-pigmentation (stars) as well non-pigmented cells (arrowhead). Scale bar: 10 μm.
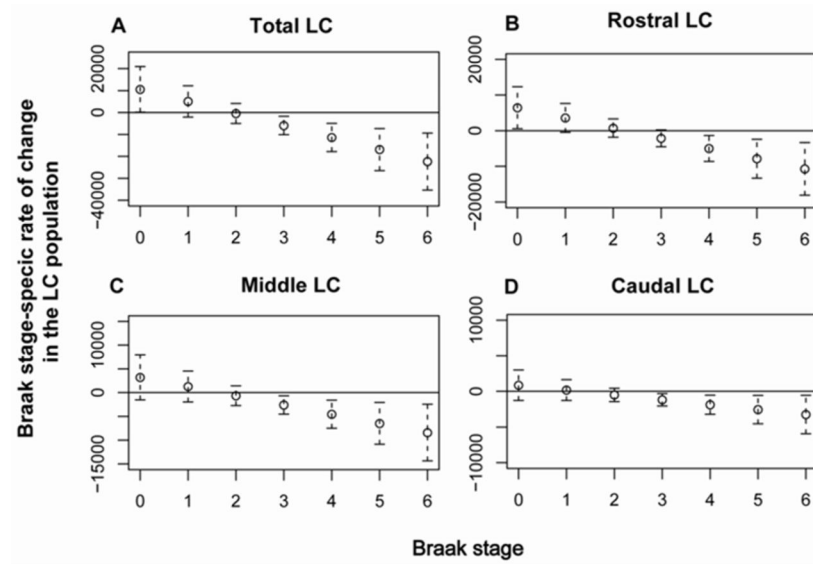
Figure 4.
Estimated Braak stage-specific rates of change in the locus coeruleus (LC) population counts per Braak stage increase (circles), along with the associated 95% confidence intervals, for total and sub-region LC population sizes. The Braak stage-specific rates of change and associated 95% confidence intervals indicate relatively constant total (A) and partial (B–D) LC population counts in Braak stages 0-II, with the rates of change not being statistically different from 0. On the other hand, the rates of change in stages III–VI are all negative and statistically significant, with an exception of the rostral LC rate (B) of change in stage III that is negative but not statistically significant at the 5% level.
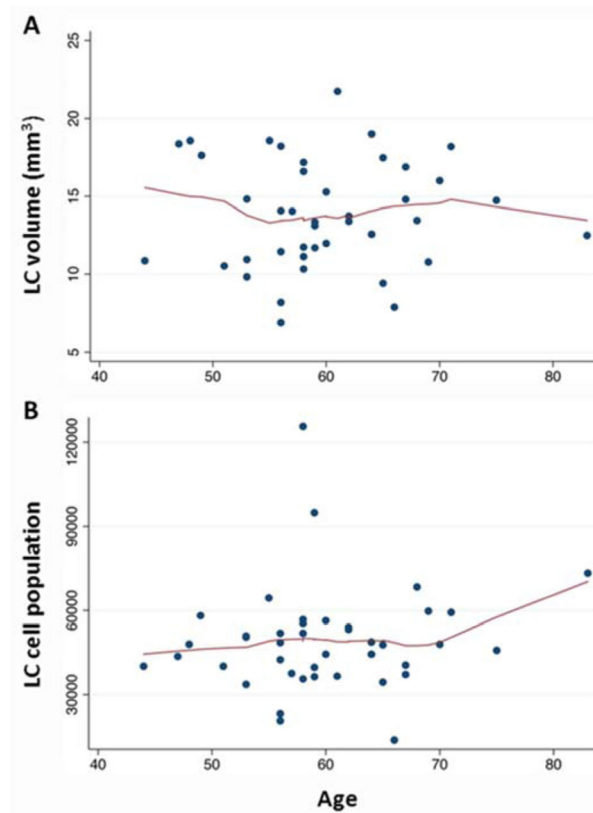
Figure 5.
The association of normal aging with total locus ceruleus (LC) volume (A) and population counts (B) among the subjects in Braak stages 0 and I was analyzed using linear regression models. The scatterplots of both LC population counts and volumes versus age indicated that both outcomes varied linearly with age so we fit regression models that included as predictors a linear term for age, as well as Braak stage, gender, and brain weight as potential confounding variables. Our analyses identified no significant changes in the LC volume and population across the age groups.

Table 1

Demographics and morphological data of the 68 cases

Subjects	Braak and Braak stage	Age (y)	Gender	Education (y)	Brain Weight (grams)	LC volume (mm3)	LC neuronal numbers	Coefficient of Error (CE) for neuronal numbers	Clinical Dementia Rating
1	0	62	F	4	1174	13.39	53,199	0.06	0
2	0	69	M	0	1506	10.78	59,722	0.06	0
3	0	62	M	11	1386	13.73	53,984	0.06	0
4	0	56	F	4	1232	11.44	48,488	0.06	0
5	0	56	M	8	1284	18.21	42,402	0.07	0
6	0	60	M	8	1392	15.28	44,365	0.07	0
7	0	49	M	0	1410	17.63	58,107	0.06	0
8	0	71	M	4	1402	18.19	59,284	0.06	0
9	0	75	M	4	1224	14.74	45,739	0.07	0
10	0	47	F	5	1202	18.37	43,580	0.07	0
11	0	64	F	0	1026	19.00	44,365	0.07	0
12	0	57	M	4	1266	14.04	37,495	0.07	0
13	0	58	M	4	1168	17.18	55,358	0.06	0
14	0	65	F	4	1020	17.48	47,702	0.06	0
15	0	48	F	0	1228	18.57	47,899	0.06	0
16	0	59	M	4	1320	11.70	39,654	0.07	0
17	0	58	M	8	1114	10.33	35,531	0.07	0
18	0	44	F	10	n/a	10.86	40,046	0.07	0
19	I	67	F	1	1114	14.80	40,439	0.07	0
20	I	64	M	4	1344	12.56	48,684	0.06	0
21	I	55	M	13	1306	18.58	64,388	0.06	0
22	I	60	F	10	1184	11.98	56,340	0.06	0
23	I	59	F	4	1304	13.11	36,317	0.08	0
24	I	59	M	8	1342	13.35	94,887	0.05	0
25	I	58	M	8	1386	11.13	56,733	0.06	0
26	I	65	F	8	1246	9.42	34,354	0.08	0

Subjects	Braak and Braak stage	Age (y)	Gender	Education (y)	Brain Weight (grams)	LC volume (mm3)	LC neuronal numbers	Coefficient of Error (CE) for neuronal numbers	Clinical Dementia Rating
27	I	58	M	4	1378	16.59	125,636	0.04	0
28	I	68	F	4	1210	13.45	68,315	0.05	0
29	I	53	M	11	1170	9.83	33,568	0.08	0
30	I	70	F	11	1242	16.01	47,899	0.06	0
31	I	83	F	n/a	1124	12.49	73,277	0.05	0
32	I	51	M	4	1458	10.52	40,046	0.07	0
33	I	67	M	11	1378	16.88	37,102	0.07	0
34	I	56	M	4	1284	8.19	23,164	0.09	0
35	I	66	F	4	1042	7.89	13,741	0.12	0
36	I	58	M	13	1216	11.74	51,825	0.06	0
37	I	56	M	11	1252	14.07	51,825	0.06	0
38	I	53	F	2	1266	10.94	50,843	0.06	0
39	I	56	F	4	1114	6.90	20,612	0.1	0
40	I	61	F	0	1212	21.75	36,513	0.08	0
41	I	53	M	15	1344	14.82	50,451	0.06	0
42	II	77	F	3	1050	11.75	61,051	0.06	0
43	II	66	F	11	1082	8.64	39,458	0.07	0
44	II	55	F	4	1134	12.63	51,629	0.06	0
45	II	68	M	11	1210	16.03	107,460	0.04	0
46	II	51	M	6	1126	8.60	25,716	0.09	0
47	II	54	M	5	1154	8.44	34,550	0.08	0
48	II	65	F	4	1238	9.27	64,781	0.06	0
49	II	63	F	4	1058	11.00	62,622	0.06	0
50	II	71	F	0	1002	21.23	71,455	0.05	0
51	II	53	M	4	1314	12.05	39,850	0.07	0
52	II	58	M	4	1346	13.90	137,910	0.04	0
53	II	46	F	6	1176	15.47	58,303	0.06	0
54	II	72	M	4	1304	8.76	35,335	0.08	0

Subjects	Braak and Braak stage	Age (y)	Gender	Education (y)	Brain Weight (grams)	LC volume (mm3)	LC neuronal numbers	Coefficient of Error (CE) for neuronal numbers	Clinical Dementia Rating
55	III	64	F	8	1152	12.19	66,940	0.06	0
56	III	66	M	4	1222	8.08	21,594	0.1	0
57	III	61	M	4	1122	12.56	52,806	0.06	0
66	III	68	F	8	1260	9.81			0
64	IV	66	M	13	n/a	13.62			0
58	V	96	F	0	1000	12.92	49,077	0.07	0
59	V	54	F	4	1202	8.91	12,760	0.12	3
60	VI	85	M	4	1304	9.53	37,691	0.07	0
61	VI	88	F	0	1052	5.81	14,527	0.12	2
62	VI	82	M	16	1133	8.51	15,116	0.12	3
63	VI	60	M	16	1140	8.01	6,674	0.17	2
65	VI	78	F	4	1080	6.76			3
67	VI	81	F	0	n/a	14.64			0.5
68	VI	70	M	18	1199	11.43			3